Assessing the onset of calcium phosphate nucleation by hyperpolarized real-time NMR

Emmanuelle M M Weber, Thomas Kress, Daniel Abergel, Steffi Sewsurn, Thierry Azaïs, Dennis Kurzbach

Assessing the onset of calcium phosphate nucleation by hyperpolarized real-time NMR

Emmanuelle M. M. Weber[a], Thomas Kress[b], Daniel Abergel[c], Steffi Sewsurn[d], Thierry Azaïs[d,*], Dennis Kurzbach[b,*]

[a] Radiological Sciences Laboratory, Department of Radiology, Stan-ford University, Richard M. Lucas Center for Imaging, 201 Welch Rd, Stanford, CA 94305, United States

[b] University Vienna, Faculty of Chemistry, Institute of Biological Chemistry, Währinger Str. 38, 1090 Vienna, Austria
E-mail: dennis.kurzbach@univie.ac.at

[c] Laboratoire des Biomolécules, LBM, Département de chimie, École Normale Supérieure, PSL University, Sorbonne Université, CNRS, 24 rue Lhomond, 75005 Paris, France

[d] Sorbonne Université, CNRS, Collège de France, Laboratoire de Chimie de la Matière Condensée de Paris (LCMCP), 4, place Jussieu, F-75005, Paris, France
E-mail: thierry.azais@upmc.fr

Abstract: We report an experimental approach for high-resolution real-time monitoring of transiently formed species occurring during the onset of precipitation of ionic solids from solution. This is made possible by real-time nuclear magnetic resonance (NMR) monitoring using dissolution dynamic nuclear polarization (D-DNP) to amplify signals of functional intermediates and is supported by turbidimetry, cryo-electron microscopy and solid-state NMR measurements. D-DNP can provide drastic signal improvements in NMR signal amplitudes, permitting dramatic reductions in acquisition times and thereby enabling to probe fast interaction kinetics such as those underlying the formation of pre-nucleation species (PNS) that precede solid-liquid phase separation. This experimental strategy allows, at unprecedented detail, for investigation of the formation of calcium phosphate (CaP)-based minerals by ^{31}P NMR - a process of substantial industrial, geological, and biological interest. So far, many aspects of the mechanisms of CaP nucleation remain unclear due to the absence of experimental methods capable of accessing such processes on sufficiently short time scales. The approach reported here aims to address this by an improved characterization of the initial steps of CaP precipitation, permitting the detection of PNS by NMR and determination of their formation rates, exchange dynamics and sizes. Using D-DNP monitoring, we find that under our conditions *i*) in the first 2 seconds after preparation of oversaturated calcium phosphate solutions, PNS with a hydrodynamic radius of $R_h \approx 1$ nm are formed; and *ii*) following this rapid initial formation, the entire crystallization processes proceed on considerably longer timescales, requiring > 20 s to form the final crystal phase.

The formation of solid calcium phosphate (CaP) phases is a highly important process in many industrial, geological and biological contexts,[1-2] and is of profound interest for fields of research ranging from mineralogy to biomineralization including bone and tooth formation.[3-4] However, despite their importance, the events occurring at the onset of CaP precipitation remain to a large extent unclear and are thus the subject of increasing research efforts. Strikingly, it was only recently that the observation of (meta-) stable so-called pre-nucleation clusters (PNC)[5] has challenged the classical nucleation and growth theory (CNT),[6] in which solid crystallized nuclei were assumed to be unstable below some critical size. Indeed, the necessity for an alternative theory of crystallisation that would account for the existence of such PNCs, described as dynamic and soluble aggregates, and rate-limiting entities (Fig. 1)[7-12], is still a matter of debate. In such a theory of non-classical crystallization pathways (NCP), PNCs constitute the first-step of a complex pathway of numerous stages (including the formation of dense liquid phases, amorphous transient intermediates and aggregation through oriented attachment) that eventually lead to the crystallized solid. This description of crystallization is often used in the field of biomineralization, particularly in cases of *in-vivo* precipitation of calcium phosphate or calcium carbonate particles with a controlled crystalline phase, size, morphology and 3D repartition. However, some authors argue that PNCs do not contradict the CNT, thereby alleviating the need of new theories.[13-16] According to this conception, stable precursors are often described as subcritical nuclei that possess a higher energetic state than the macroscopic crystal (>1 micron) but that remain in thermodynamic equilibrium with the solution. [13-16]
However, the important point is that, regardless of the theory, the structure and the dynamic behavior of precursor species remain poorly understood, and the factors that control the associated nucleation events remain unclear, leaving significant gaps in the current understanding of crystallization.[17]
While PNC typically denotes a stable or metastable nanometric solute, we herein term pre-nucleation species or (PNS) any CaP aggregate that occurs in solution during the early onset of CaP precipitation. This will ensure sufficient generality to our conclusions by avoiding any reference to a particular nucleation or crystallization theory (CNT or NCP). In this sense, the PNS terminology introduced here should be understood as neutral. This distinction is all the more important as the concepts of nucleation theories and crystallization pathways can be used to describe different processes.
PNS are here understood as nanometeric solutes constituted of loosely coordinated ions in dynamic equilibrium with the corresponding free solvated species. Recently, PNS have been categorized by Zahn[11] into two types, which we here denote as *i*) *Type 1 PNS*, (corresponding to PNC)[5], which are stable or metastable in solution and only participate in precipitation upon receiving further stimuli; and *ii*) *type 2 PNS*, which appear transiently during the onset of the phase separation event[8] and which are notoriously challenging to detect and characterize due to their limited life-times. This distinction is retained here, although type 1 and 2 PNS may (or may not) share similar structural and dynamic properties – a point that remains to be investigated.

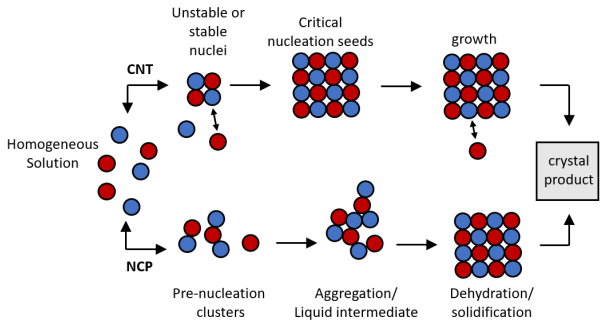

Figure 1. Distinction between classical (CNT, top) and non-classical crystallization pathways (NCP, bottom) as adapted from the work by Gebauer and Wolf.[8] In the classical picture, materials are often depicted to crystallize via nucleation of critical crystalline seeds and subsequent growth through ion-by-ion attachment. In contrast, NCP descriptions often assume (meta)stable pre-nucleation clusters that persist in solution, prior to their aggregation into amorphous solids or liquid transient intermediates and their subsequent precipitation. While the classical pathway is thermodynamically controlled, the NCP is thought to be dynamically controlled to a large degree.[8]

Among other examples, type 1 PNS have been observed to be stable in solutions of calcium phosphate,[18] calcium carbonate[5] or iron (oxyhydr)oxides.[12] However, in the case of calcium phosphates, only a small number of studies[18-20] report direct experimental evidence of PNS, despite their importance for the understanding of bone biomineralization, where anomalous mineral formation might impact some bone pathologies (*e.g.*, Paget's disease).[21] Regarding type 2 PNS, experimental observations are even scarcer. Indeed, only Habraken et al.[9] have reported such data. This lack of experimental data warrants deeper investigation.

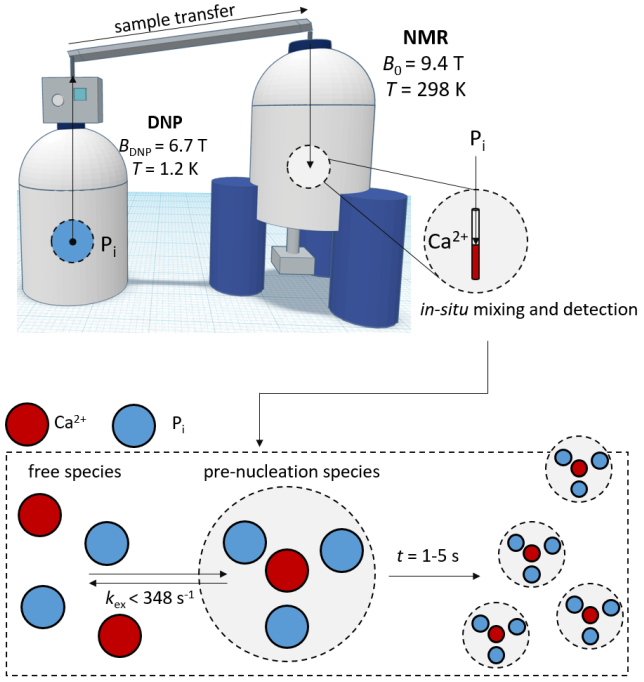

Figure 2. Schematic representation of the experimental setup for real-time monitoring of CaP PNS formation by D-DNP. Inorganic phosphate P_i is hyperpolarized by DNP at 1.2 K to boost the ^{31}P NMR magnetization. The hyperpolarized sample is then rapidly dissolved and transferred to an NMR spectrometer where it is mixed *in-situ* with a Ca^{2+}-containing solution. After mixing, free and PNS-bound P_i are in dynamic equilibrium, while the PNS formation is monitored in real time. The process takes place on a 1-5 s time scale at 25°C and pH 7.8.

To help answering to the current need for insights into PNS, we introduce here an experimental strategy that can provide insight into the very early stage of the CaP formation with high temporal as well as atomistic resolution. Our approach targets two different aspects of the process: *a*) Atomic-level details of the initial stages of CaP formation including the first detection of type 2 PNS by NMR - providing a microscopic perspective on PNS formation to confirm the existence of type 2 PNS, and if successfully observed, track their behavior; *b*) Characterization of the evolution of the collective solution/precipitate system, providing a complementary macroscopic perspective on the phase separation process.

The proposed methodology employs dissolution dynamic nuclear polarization (D-DNP, Fig. 2), a technique for obtaining drastically signal-enhanced nuclear magnetic resonance (NMR) spectroscopy[22-24], used to detect, monitor and characterize PNS formation (point (*a*)). The D-DNP NMR results are supplemented by real-time turbidity measurements, cryo-electron microscopy, and solid-state NMR, to gain complementary access to larger CaP aggregates and solid precipitates (point (*b*)).

Experimental Section

D-DNP

250 µL of a P_i solution (100 mM TRIS buffer at pH 7.8) supplemented with 50 mM of TEMPOL and mixed 1:1 v/v with glycerol-d_8 as cryo-protectant (yielding a final P_i concentration of 0.5 M) was hyperpolarized at a temperature of 1.2 K in a magnetic field of 6.7 T during 1.5 h in a prototype of a Bruker DNP polarizer. The microwave frequency was set to either 187.90 GHz (positive DNP) or 188.38 GHz (negative DNP) and modulated at 1 kHz with a saw tooth function over a bandwidth of 100 MHz.[25]

The hyperpolarized sample was then dissolved by a burst of 5 mL (hence diluted 20-fold to a P_i concentration of 25 mM) superheated D_2O at 180°C and 10.5 bar and propelled through a 0.9 T "magnetic tunnel"[26] by pressurized helium at 7 bar within 4 s to a 9.4 T Bruker Avance II NMR spectrometer where it was mixed (in less than 1 s) 4:1 v/v with 500 mL TRIS buffer (yielding 20 mM P_i) containing 0, 8 or 13 mM $CaCl_2$ (final concentration) at 298 K. The final volume was 2.5 mL. The spectrometer was not field-frequency locked to allow the detection to start as soon as possible. After dissolution and mixing the resulting pH was determined to be 7.8±0.2.

Detection was achieved at intervals of 0.5 s by applying non-selective 30° pulses with a ^{31}P carrier frequency set to 0 ppm. The spectral width was 40 ppm using a 10 mm BBO probe.

All data were analyzed using home-written MATLAB scripts. All spectra were apodised with Gaussian window functions. Signal intensities were extracted by adapting a strategy published before[27-30] using a Lorentzian fit implemented in the 'fit' function of MATLAB. The scripts employed the GNAT and EasySpin tool boxes for data loading and apodization.[31-32]

To extract the kinetic rates from the D-DNP experiments, the signal intensity time traces were fitted to the following functions for mono- and bi-exponential behavior respectively:

$$S(t) = S_0 \exp(-R_{DEC} t) + S_{eq} \quad (1)$$

$$S(t) = (S_0' \exp(-R_{DEC} t) - S_0'' \exp(-R_{UP} t)) + S_{eq} \quad (2)$$

Where $S(t)$ is the signal amplitude at time point t after mixing, S_0' and S_0'' fixed signal amplitudes of the build-up and decay

functions to modulate the bi-exponential behavior and S_{eq} the equilibrium signal amplitude for longer times.
The time traces were fitted using the bisquare method as implemented in the MATLAB curve fitting tool. Note that R_{DEC} does not equal R_1 but includes all causes of phenomenological signal loss.

Turbidimetry
Turbidimetry measurements were performed with a home-built turbidimeter using a SEN0189 turbidity sensor and a home-written Arduino control system. The experiments were performed at room temperature and the sampling rate was 1 s^{-1}.

Cryo-EM
After mixing of phosphate and $CaCl_2$ solutions under similar concentrations as in the D-DNP experiments (13 mM Ca^{2+}), the specimens were frozen as fast as possible by plunging into liquid ethane cooled by liquid nitrogen (LEICA EM CPC, Vienna, Austria). The delay between sample preparation and freezing was ca. 15-30 s. The cryofixed specimens were mounted into a Gatan cryoholder (Gatan inc., Warrendale, PA) for direct observation at 93 K (-180 °C) in a JEOL 2100HC cryo-TEM operating at 200 kV with a LaB6 filament. Images were recorded in zero-loss mode with a Gif Tridiem energy-filtered-CCD camera equipped with a chip with 2k x 2k pixels (Gatan Inc., Warrendale, PA). Acquisition was accomplished with Digital Micrograph software (versions 2.31.734.D, Gatan inc., Warrendale, PA).

SS NMR
Solid-state nuclear magnetic resonance (NMR) experiments were conducted using an Avance-III 300 Bruker spectrometer. Precipitates were produced with a concentration of [Ca^{2+}] = 13 mM, were packed into 4 mm (O.D.) zirconia rotors, and experiments were conducted using magic angle spinning (MAS). The spinning frequency was ν_{MAS} = 14 kHz using a Bruker 4BL CP/MAS ^{1}H/BB probe. The recovery delays for ^{1}H relaxation were set to 10 s. A two-dimensional ^{1}H-^{31}P heteronuclear correlation spectrum was recorded with 128 t_1 increments with 40 transients each. The cross-polarization (CP) contact times were set to t_{CP} = 3 ms. Proton chemical shifts were referenced to TMS at 0 ppm, whilst ^{31}P chemical shifts were referenced to H_3PO_4 (85% w/w aqueous solution) at 0 ppm.

Estimation of the PNS radius
Under the assumption of a simple isotropic rotation of the PNS, the transverse relaxation rate of an isolated ^{31}P spin depends on its CSA $\Delta\sigma$ according to[15]:

$$R_2 = \frac{1}{15}(\gamma_i B_0 \Delta\sigma)^2 \left[\frac{4}{3}\tau_c + \frac{\tau_c}{1+(\omega_L\tau_c)^2}\right] \quad (3)$$

where γ_i denotes the gyromagnetic ratio of nucleus *i*, B_0 static the magnetic field, ω_L the Larmor frequency and τ_c the rotational correlation time. In the extreme narrowing limit where $\omega_L \gg \tau_c$, eq. 1 reduces to:

$$R_2 = \frac{7}{3}\frac{1}{15}(\gamma_i B_0 \Delta\sigma)^2 \tau_c \quad (4)$$

The effective hydrodynamic radius R_h can be calculated according to the Stokes-Einstein relation:

$$R_h = \sqrt[3]{\frac{3kT\tau_c}{4\pi\eta}} \quad (5)$$

Where k denotes the Boltzmann constant, T the temperature and η the dynamic viscosity. It follows that

$$R_h^3 = \frac{3kT}{4\pi\eta} C R_2 \quad (6)$$

With the constant

$$C = \frac{7}{6}\frac{15}{2}(\gamma_i B_0 \Delta\sigma)^{-2} \quad (7)$$

For free P_i in the absence of Ca^{2+}, we determined that $R_2(P_i)$ = 5.3 s^{-1} under our experimental conditions by conventional spin-echo experiments. Assuming a CSA of 68 ppm (as reported for brushite)[33] for ^{31}P in a PNS and 3 $\Gamma_2(P_i) = \Gamma_2(P_{PNS}) > R_2(P_{PNS})$ as explained in the main text, eqs. 3-7 yield $R_h < 0.94$ nm for the PNS. Note that this value is an estimate and must be interpreted with care.
All linewidths have been determined after stabilization of the sample, *i.e.* 2 s after completion of the mixing processes to avoid biases due to shim instabilities (see Supplementary Material Figs. S3-S5).

Results and Discussion

1. The birth of a mineral witnessed by D-DNP

By combining D-DNP with real-time NMR measurements, we have developed the capability to directly observe and analyze transient PNS that may be present immediately after preparation of oversaturated CaP solutions. In our hands, such signals remained below the detection threshold of conventional NMR (see Supplementary Material Fig. S1), in the absence of signal enhancement by D-DNP. D-DNP amplifies NMR signals of various substrates through a "hyperpolarization" procedure (Fig. 2) that consists of *i)*. microwave irradiation of a sample that contains a paramagnetic polarization agent (PA; here 50 mM TEMPOL) in a magnetic field ($B_{0,DNP}$ = 6.7 T) at cryogenic temperatures (T_{DNP} = 1.2 K), followed by *ii)* rapid heating and dissolution of the sample, and *iii)* the transfer (with a transfer time $t_{transfer}$ = 4 s) of the hyperpolarized sample to a liquid-state NMR spectrometer for detection ($B_{0,NMR}$ = 9.4 T at T_{NMR} = 298 K).

Our strategy for real-time monitoring of CaP formation is thus based on *i)* the production of hyperpolarized phosphate (P_i) followed by *ii)* sample dissolution and rapid mixing with a Ca^{2+}-containing solution *in-situ* in an NMR spectrometer, and *iii)* the time-resolved detection of NMR spectra of hyperpolarized ^{31}P nuclei, which reports on the presence of PNS and on the local phosphate environments (see Fig. 2). This strategy allows one to monitor the P_i interaction with Ca^{2+} on a time scale of a few seconds immediately after mixing of the two interacting components. For the case at hand, NMR real-time monitoring was achieved using a single pulse-acquisition scheme applied at a rate of 2 s^{-1} and a flip angle of 30°. Comparable strategies by Katz-Brull and co-workers[34] have already shown their value in medicinal contexts.

The observation of PNS on timescales of ca. 10 s was made possible with a D-DNP prototype system, which enables complete mixing of the two components within ca. 1 s upon arrival of the P_i solution in the NMR tube. NMR detection was initiated only upon completion of the mixing process.

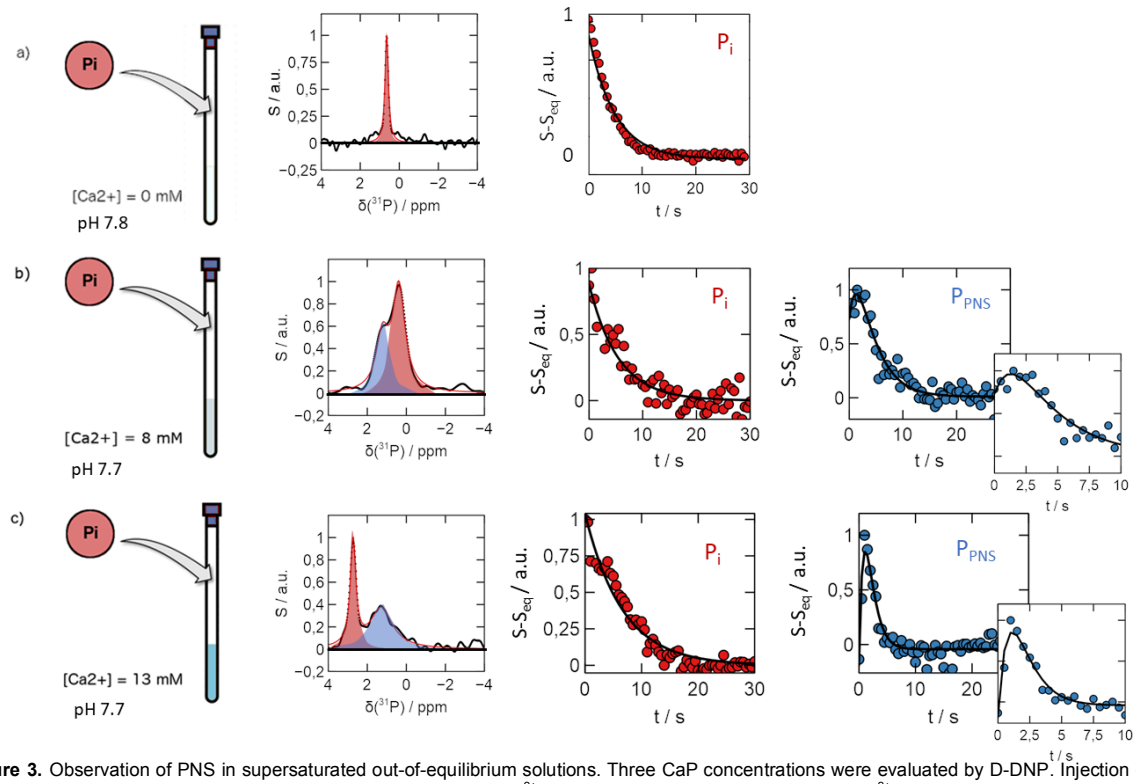

Figure 3. Observation of PNS in supersaturated out-of-equilibrium solutions. Three CaP concentrations were evaluated by D-DNP. Injection of a P_i solution into (a) pure buffer (concentrations: [Pi] = 20 mM; [Ca^{2+}] = 0 mM), (b) & (c) into a solution of Ca^{2+} (concentrations: [Pi] = 20 mM; [Ca^{2+}] = 8 & 13 mM; all concentrations are final concentrations in the NMR tube after mixing). a) Centre: a single P_i signal is seen which is indicative of the free Pi in solution. Right: evolution of the ^{31}P NMR signals after mixing at t = 0 at a calcium ion concentration of [Ca^{2+}] = 0, and T = 298 K. The signal intensity decreases exponentially towards thermal equilibrium after mixing. b) Centre: At a concentration of [Ca^{2+}] = 8, pH 7.8 and T = 298 K two signals appear, one corresponding to free P_i (red) and a second indicating phosphate interacting with calcium (P_{PNS}; blue). Right: Signal intensity of free Pi and P_{PNS}. While the former decrease monotonically to equilibrium, the signal of P_{PNS} builds up during the first 2.5 s after mixing before it decays to naught as a consequence of relaxation and growth/aggregation of the PNS. c) A similar behaviour as in b) is observed at a concentration of [Ca^{2+}] = 13, and T = 298 K, but the line of free Pi shifts to the left of the PNS signal (see main text). pH values after mixing are indicated. The signal intensities were referenced to their equilibrium signal intensities S_{eq} at t →∞.

First, we analyzed the dependence of the hyperpolarized phosphate spectra on the Ca^{2+} concentration (denoted [Ca^{2+}]) directly after *in-situ* mixing. Fig. 3 displays ^{31}P spectra obtained within 2 s the mixing of 20 mM hyperpolarized P_i with solutions of varying Ca^{2+} concentration (concentrations given after mixing). In the absence of any Ca^{2+} ions, a single narrow signal is observed at $\delta(^{31}P)$ = 0.7 ppm with a linewidth of $\lambda(P_i)$ = 35.2±6.9 Hz. This signal decays monotonically with time and can be considered as fingerprint of free, hyperpolarized P_i in solution under our conditions. This is in contrast to the spectra observed in the presence of Ca^{2+} ([Ca^{2+}] = 8 mM and 13 mM).

For [Ca^{2+}] = 8 mM resonances were detected at $\delta(^{31}P)$ = 0.6 ppm and 1.6 ppm. The signals were fitted to Lorentzian line shapes of $\lambda(P_i)$ = 129.5±4.1 and 128.3±8.0 Hz. These two lines were assigned to free P_i (high-field signal) and to phosphate interacting with Ca^{2+} ions (low-field signal). The signal of free P_i was identified by its monotonic decay after mixing, while the signal of the Ca^{2+}-binding species initially grows (characteristic for the formation of CaP species) before decreasing to naught. (See Section 2 for details.)

At a calcium ion concentration of [Ca^{2+}] = 13 mM, again two peaks appear, although with different chemical shifts ($\delta(^{31}P)$ = 1.3 for free and 2.7 ppm for bound P_i) and different linewidths ($\lambda(P_i)$ = 233.4±5.8 Hz and 58.1±4.4 Hz). The signal for free P_i is again characterized by a monotonic decay, while PNS-bound phosphate shows the characteristic build-up and decay behavior indicative of Ca^{2+}-interaction.

1a. Line shape Analyses

The D-DNP results provide key information about two distinct aspects of PNS formation: *i*) the size and motional freedom of the developing solute species (via the ^{31}P linewidths); and *ii*) on the phosphate exchange rate (via the number of ^{31}P signals observed):

i) linewidth-based information – determination of PNS size: In liquid-state NMR spectroscopy, the homogeneous linewidth of a signal is proportional to the intrinsic transverse relaxation rate of the nuclear spin R_2, which in turn depends on the correlation time τ_c of rotational diffusion of the spin-bearing moiety. It is therefore likely that the observed similar linewidths at [Ca^{2+}] = 8 mM indicate that both free and interacting species have comparable rotational diffusion properties, despite their different chemical shifts that indicate distinct chemical environments. In contrast, the differing linewidths at [Ca^{2+}] = 13 mM suggest that the Ca^{2+}-interacting species takes part in the formation of a cluster that is significantly larger than free P_i. However, for the case at hand, we only compare relative linewidths within a single detection (to avoid biases due to shim instabilities etc.) and measure the sum Γ of homogeneous and inhomogeneous linewidths. Therefore, we can only state that $R_2 < \Gamma$. Under the assumption of fast rotational diffusion of a spherical particle, where $R_2 \propto \tau_c$ holds, a three-fold broader line, as observed for the broad signal at [Ca^{2+}] = 13 mM (Fig. 3), indicates at most a three-fold longer rotational diffusion time, corresponding to a maximum increase by a factor $3^{1/3}$ (≈ 1.4) of the hydrodynamic radius R_h according to the Stokes-Einstein equation. This enables an estimate of R_h < 0.9 nm for the hydrodynamic radius of the transiently observed Ca^{2+}-binding P_i species that we

detect here during the onset of calcium phosphate precipitation. The inequality takes all exchange processes and other inhomogeneous broadening effects into account (cf. Materials and Methods) It should be noted that concentration-dependent chemical exchange is a well-documented property of metal-ligand complexes and of many biological systems, such as the exchange of lipids between vesicles[16] or of DNA-transcription factor complexes.[17,18] A comparable concentration-dependence could here contribute to the growing line width upon increasing Ca^{2+} ion concentrations. Indeed, growing counter ion concentrations might accelerate the exchange between free and PNS-bound phosphate species thereby broadening the ^{31}P resonances.

On the short time scales of the D-DNP experiments, it is yet complicated to assess the exchange rates of the species corresponding to the individual lines, as signal averaging and mixing time incrementation are hardly feasible. A possible way to obtain exchange rates would be the use of ultrafast exchange spectroscopy (*i.e.* single scan approaches combined with EXSY/NOESY) as proposed in combination with D-DNP by Swisher et al.[35]

Nevertheless, our finding is in agreement with the estimated radius of stable type 1 PNS reported by Dey et al.[18] (0.44 nm) and of type 2 PNS reported by Habraken et al.[36] (0.45 to 0.65 nm), who both found that this size would be consistent with PNS composed of three phosphate units. We therefore conclude that we directly observe nanoscopic objects that emerge during the onset of the precipitation of calcium phosphate in oversaturated solutions, *i.e.* type-2 PNS which are constituted of at most 3 phosphate units and (henceforth denoted P_{PNS}).

It should be noted that the chemical shift of free P_i changes in our hands when varying the Ca^{2+} concentration. This might be a consequence of relatively low buffer concentrations and counter ion effects in solution including the variation of the ionic strength.[37] The analyses presented above however hold, as they are not affected by this fact. Further reference data for the line shape analysis is included in the Supplementary Material (Fig. S2-S5).

ii) Chemical shift-based information – determination of dynamic exchange rates: At $[Ca^{2+}]$ = 8 and 13 mM, the simultaneous presence of two separate signals indicates that the exchange rate (k_{ex}) of P_i between its free (P_i) and bound forms (P_{PNS}) is slow on the NMR timescale, *i.e.* $k_{ex} < \Delta\nu$, where $\Delta\nu$ denotes the difference in resonance frequencies of the two signals. The upper bound of the exchange rate at the two concentrations can thus be estimated to be 249 and 348 s^{-1}, respectively.

1b. Real-time analyses

In addition to the information contained in static PNS spectra, real-time detection in D-DNP experiments provides key insights into the kinetics of PNS formation.

Fig. 3a to c (middle and right panels) show time traces of the NMR signal intensities of free P_i (red) as well as P_{PNS} (blue) when present. At all tested Ca^{2+}-concentrations, the signal intensity of free phosphate decays exponentially, primarily due to the return of the hyperpolarized ^{31}P spins to thermal equilibrium. At 8 mM ≤ $[Ca^{2+}]$ ≤ 13 mM, the observed Ca^{2+}-interacting species P_{PNS} though displays a build-up of signal intensity during the first 2 s after mixing. The P_{PNS} signal intensity here reports on the presence of Ca^{2+}-interacting phosphate and thus on the formation of PNS. The build-up starts directly after mixing of the two components so that a significant PNS signal could be detected already 0.5 s after mixing. This is then followed by a decay and eventual disappearance of the signal. In addition to the return to thermal equilibrium of the hyperpolarized ^{31}P spins, the P_{PNS} signal may also decay for t > 2 s if the growth or aggregation of the PNS generates species with molecular weights that are too high to allow detection by solution-state NMR (*i.e.* post-nucleation species). No P_{PNS} signal could be detected in the time-series after 10 s at $[Ca^{2+}]$ = 8 mM, and after 5 s at $[Ca^{2+}]$ =13 mM.

The time traces of the P_i and P_{PNS} signals could be fitted respectively to mono-exponential (decay only) and bi-exponential (build-up followed by decay) functions. Both decreasing functions account for all sources of signal loss (growth, conversion, rf pulses, paramagnetic relaxation etc.) by a single rate constant R_{DEC}. Therefore, in case of bi-exponential behavior, the build-up rate R_{BU} reflects only the formation of PNS-bound phosphate. Table 1 lists the obtained decay rates R_{DEC} and build-up rate constants R_{BU}. Importantly, R_{BU} *relates to the kinetics of PNS formation* as the signal growth corresponds to the formation rate of Ca^{2+} interacting phosphate species.

The P_i decay rates are largely independent of the Ca^{2+} concentration showing that longitudinal relaxation is not strongly impacted by varying ionic strength. Similarly, the P_{PNS} build-up rates, R_{BU}(PNS), are constant within the error margin. Thus, under our conditions the rate of PNS formation appears to be independent of the Ca^{2+} concentrations. In contrast, the variation of the R_{DEC}(PNS) values reflects a dependence of post-nucleation aggregation as well relaxation processes on $[Ca^{2+}]$. Indeed, the higher the Ca^{2+} concentration the faster the decay rate indicating accelerated aggregation at elevated counter ion quantities (cf. turbidimetry data in section 2).

Table 1. Characteristic decay rates R_{DEC} and build-up rates R_{BU} observed in the D-DNP experiments. (The Methods section contains details on the fitting procedure.)

Concentrations	Decay and build-up rates
$[P_i]$ = 20 mM $[Ca^{2+}]$ = 0 mM	$R_{DEC}(Pi)$ = (0.19±0.02) s^{-1}
[Pi] = 20 mM $[Ca^{2+}]$ = 8 mM	$R_{DEC}(Pi)$ = (0.19±0.03) s^{-1} **$R_{DEC}(PNS)$ = (0.28±0.16) s^{-1}** **$R_{BU}(PNS)$ = (0.66±0.71) s^{-1}**
[Pi] = 20 mM $[Ca^{2+}]$ = 13 mM	$R_{DEC}(Pi)$ = (0.15±0.02) s^{-1} **$R_{DEC}(PNS)$ = (0.92±0.32) s^{-1}** **$R_{BU}(PNS)$ = (0.95±0.30) s^{-1}**

It should be mentioned that the D-DNP approach employs additives such as glycerol and the polarizing agent (TEMPOL). These specific conditions might influence the precipitation process, which therefore cannot directly be compared to previously published data on CaP systems.

2. The Macroscopic Phase Transition

To compare the atomistic perspective that D-DNP provides with a macroscopic picture that includes the entire Ca^{2+}/P_i/buffer system, we performed real-time turbidimetry experiments to monitor the precipitation events. These experiments provided observations of the aggregation processes occurring within 10 and 20 s (depending on the Ca^{2+} concentrations), whereas the PNS NMR signal peaked 2 s after mixing in the D-DNP

experiments. This suggests that significant amounts of type 2 PNS can only be found during the onset of the event, although the macroscopically observable phase separation process takes longer.

However, it should be considered that the NMR signal decay is in part determined by relaxation effects. Therefore, the faster decay of the NMR signals in the D-DNP experiments as compared to the turbidity curves does not necessarily prove that the corresponding species also disappear faster. Instead, they might persist for longer periods, yet remain invisible to NMR experiments as a consequence of rapid longitudinal relaxation.

The curves in Fig. 4a represent the intensity of light that passes through the NMR sample tube after *in-situ* mixing of P_i- and Ca^{2+}-containing solutions (20 mM P_i, 0, 10 or 20 mM $CaCl_2$). CaP particle growth after mixing leads to visible light scattering, as seen by the decreasing sample transparency. We thereby observed a phase transition event within ~10 or 20 s, for calcium ion concentrations of 10 or 20 mM, respectively. In contrast, the P_{PNS} signals observed by D-DNP dropped to zero after 5 or 10 s, respectively.

Hence, PNS, *i.e.* nanoscale inhomogeneities that initiate the CaP precipitation event, might be associated with the early stage of the process, while nucleation can be associated with later stages. Similar convergence between nanoscale inhomogeneities that precede macroscopic phase transitions is well documented in the field of polymer physics.[38-40] For example, stimuli-responsiveness of polymers is based on nanoscale inhomogeneities that precede the gelation of a polymer solution and often determine the cooperativity of such transitions.[40] Possibly, a similar conjunction might be witnessed here in the context of CaP formation. This is also in agreement with the convergence of classical and non-classical crystallization theories that has been proposed by Habraken et al.[9]

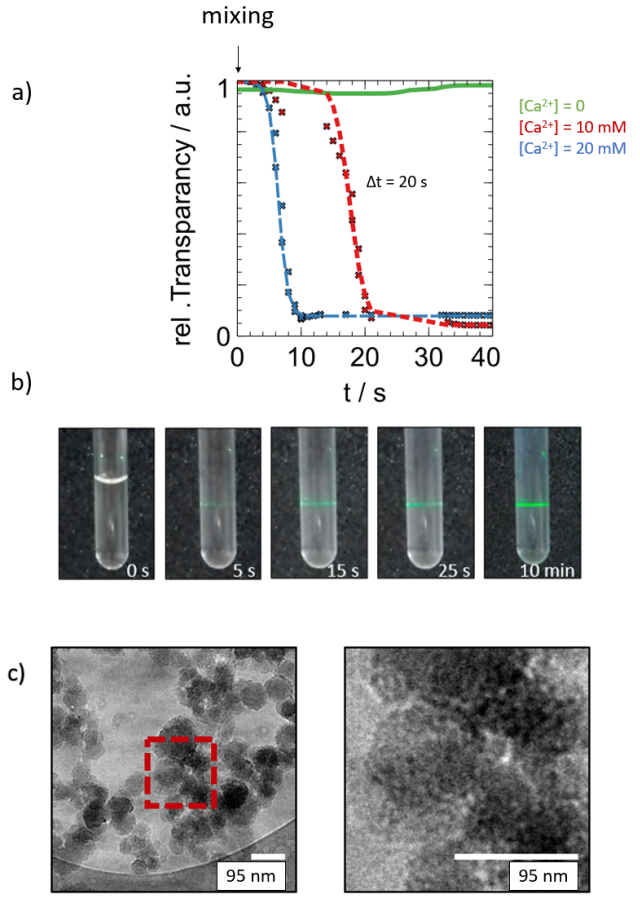

Figure 4. Macroscopic observations of CaP precipitation. a) Turbidimetry experiments expressed as time dependence of light transmissibility (detected intensity) of CaP solutions after mixing of 20 mM P_i with different concentrations of Ca^{2+} ions. By this means the phase transition was observed to take 10-20 s depending on the Ca^{2+} concentration (grey shade). The higher the Ca^{2+} concentration, the faster the precipitation. Note that in agreement with the D-DNP data, the precipitation event proceeds faster at higher Ca^{2+} concentrations. b) Temporal evolution of the NMR sample tube after mixing of P_i and Ca^{2+}. Within 10 min., macroscopic precipitates cause light to scatter. Even within the first 5 s, *i.e.* during the period accessible for D-DNP, light scattering was already observed. c) Cryo-electron micrographs confirm the presence of ~ 100 nm large CaP cluster ca. 30 seconds after mixing of the two phosphate and calcium chloride solutions. The red box indicates the area magnified on the right. The amorphous clusters feature an internal architecture due to aggregation of smaller particles of ca. 5-10 nm.

Therefore, to corroborate the turbidity data, Fig. 4b illustrates how a green laser beam is scattered only 5 s after *in-situ* mixing of P_i and Ca^{2+}-containing solutions in the NMR sample tube. This hints towards aggregates of several hundreds of nanometers, which are too large to be detected by liquid state NMR yet accessible by turbidimetry already a few seconds after mixing. It appears therefore reasonable to assume that aggregation of PNS plays a large role in the disappearance of the NMR signals and that relaxation alone cannot account for the rapid signal disappearance. This interpretation would also explain why PNS could only be detected during the first ~5 s after mixing by D-DNP, although the entire precipitation process takes ca. 10-20 s, judging from the turbidity experiments. We want to stress that the particle size should be interpreted with care though, as turbidity can be correlated with particle size distributions only in combination with further X-ray or light scattering data.

Cryo-electron microscopy (EM) experiments (Fig. 4c) confirmed the presence of large (~ 100 nm) CaP amorphous particles already 30 seconds after initiation of the precipitation event. Interestingly, they display an internal structure made of smaller particles (ca. 5-10 nm). These observed structure might nevertheless stem from aggregation of secondary particles composed of PNS. Indeed, a pathway cannot be excluded that explains the disappearance of PNS (as detected by D-DNP) by aggregation of particles through secondary nucleation as it has been described for ACC precipitation[13].

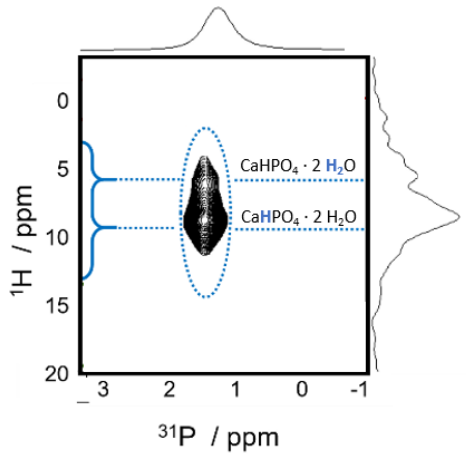

Figure 5. Solid-state NMR spectrum (HETCOR) of the final precipitate. A brushite-only structure was observed, which includes 2 water molecules per phosphate unit. The solid was recovered by centrifugation form the final mixture of the D-DNP experiments, 10 min. after mixing of the two interactants.

Finally, solid-state NMR measurements revealed the final crystallographic phase following the real-time experiments. We determined the internal architecture of crystallites formed 10 min minutes after mixing by means of solid-state ^{1}H-^{31}P heteronuclear correlation (HETCOR) spectroscopy.[41-42] The spectrum in Fig. 5 features characteristic resonances of $CaHPO_4{\cdot}2H_2O$, *i.e.* of brushite crystals. Such spectra remained unchanged for 2 days after sample preparation.

Notably, the spectrum in Fig. 5 displays a brushite-only internal architecture with two well-defined peaks stemming from the two types of protons within the crystalline phase (*i.e.* $\mathbf{H}_2O$ and $\mathbf{H}PO_4^{2-}$). Hence, starting from solute PNS that form on a time scale of a few seconds, macroscopic brushite crystallites emerge on longer timescales to shape the final product. The system thereby undergoes a disorder-to-order transition from nanoscale inhomogeneities (observed after 0.5 - 8 s) to macroscopic crystals (observed after 10 min - 2 h) on a seconds-to-minutes timescale.

Conclusions

We present an experimental spectroscopic strategy that enables the analysis of the initial phases of mineral precipitation events and that reports on PNS size and kinetics, ion exchange rates as well as macroscopic phase behavior and the architecture of the final solid.

As PNS are currently assumed to constitute the first step in precipitation and growth of crystalline CaP, their rate of formation is possibly defining the growth-rate limiting factor that determines the kinetics of CaP precipitation from aqueous solution. Real-time monitoring of PNS formation by D-DNP allows one to obtain key information about these important nanoscopic entities. The method is here reported with an example to CaP formation in a biomineralization context, yet wide ranges of concentrations, pH and temperatures as well as other systems (*e.g.* carbonate, silicate or nitrate) are in principle accessible on time scales ranging from milliseconds up to several minutes.

By integrating real-time techniques with microscopy and solid-state measurements many aspects of the precipitation of CaP from aqueous solution could be captured, from the formation of initial PNS to the final precipitate.

Based on NMR, our approach capitalizes on an intrinsically high (atomistic) resolution and adds a temporal dimension to this method's portfolio - an approach that might prove valuable for the investigation of transient intermediates, precipitation events and interaction monitoring in general and that should have a widespread potential to monitor structure and kinetics of functional intermediates in the contexts biomineralization and crystallization.

Supporting Information

D-DNP reference experiments; fitting results for real-time D-DNP experiments.

Acknowledgements

The authors thank Mrs. Ludovica M. Epasto, Mrs. Estelle Loh as well as the entire D-DNP team at LBM (and in particular to: Dr. M. Baudin, Prof. G. Bodenhausen, Mr. D. Guarin, MSc.) for its continuous support. This research was supported by the French Centre National de la Recherche Scientifique (CNRS), the European Research Council (ERC contract 'HYPROTIN', grant agreement 801963). The authors thank Bruker BioSpin for providing the D-DNP equipment and the EM Service of the IBPS (CNRS FR 3631) at UPMC. The authors thank the Cluster of Excellence MATISSE led by Sorbonne Universités.

Keywords: Dissolution DNP • Calcium Phosphate Crystallization • Prenucleation Species • NMR Spectroscopy • Biomineralization

References

1. LeGeros, R. Z., Calcium phosphate-based osteoinductive materials. *Chem Rev* **2008,** *108* (11), 4742-53.
2. Wang, L. J.; Nancollas, G. H., Calcium Orthophosphates: Crystallization and Dissolution. *Chem Rev* **2008,** *108* (11), 4628-4669.
3. Habraken, W.; Habibovic, P.; Epple, M.; Bohner, M., Calcium phosphates in biomedical applications: materials for the future? *materialdtoday* **2015,** *19*, 69-87.
4. Glimcher, M. J., Bone: Nature of the calcium phosphate crystals and cellular, structural, and physical chemical mechanisms in their formation. *Rev Mineral Geochem* **2006,** *64*, 223-282.
5. Gebauer, D.; Volkel, A.; Colfen, H., Stable prenucleation calcium carbonate clusters. *Science* **2008,** *322* (5909), 1819-22.
6. Karthika, S.; Radhakrishnan, T. K.; Kalaichelvi, P., A Review of Classical and Nonclassical Nucleation Theories. *Cryst. Growth Des.* **2016,** *11*, 6663-6681.
7. Demichelis, R.; Raiteri, P.; Gale, J. D.; Quigley, D.; Gebauer, D., Stable prenucleation mineral clusters are liquid-like ionic polymers. *Nature Communications* **2011,** *2*.
8. Gebauer, D.; Wolf, S. E., Designing Solid Materials from Their Solute State: A Shift in Paradigms toward a Holistic Approach in Functional Materials Chemistry. *J Am Chem Soc* **2019,** *141* (11), 4490-4504.
9. Habraken, W. J.; Tao, J.; Brylka, L. J.; Friedrich, H.; Bertinetti, L.; Schenk, A. S.; Verch, A.; Dmitrovic, V.; Bomans, P. H.; Frederik, P. M.; Laven, J.; van der Schoot, P.; Aichmayer, B.; de With, G.; DeYoreo, J. J.; Sommerdijk, N. A., Ion-association complexes unite classical and non-classical theories for the biomimetic nucleation of calcium phosphate. *Nat Commun* **2013,** *4*, 1507.
10. Dorvee, J. R.; Veis, A., Water in the formation of biogenic minerals: peeling away the hydration layers. *J Struct Biol* **2013,** *183* (2), 278-303.
11. Zahn, D., Thermodynamics and Kinetics of Prenucleation Clusters, Classical and Non-Classical Nucleation. *Chemphyschem* **2015,** *16* (10), 2069-2075.
12. Scheck, J.; Wu, B.; Drechsler, M.; Rosenberg, R.; Van Driessche, A. E.; Stawski, T. M.; Gebauer, D., The Molecular Mechanism of Iron(III) Oxide Nucleation. *J Phys Chem Lett* **2016,** *7* (16), 3123-30.
13. Carino, A.; Testino, A.; Andalibi, M. R.; Pilger, F.; Bowen, P.; Ludwig, C., Thermodynamic-Kinetic Precipitation Modeling. A Case Study: The Amorphous Calcium Carbonate (ACC) Precipitation Pathway Unravelled. *Crystal Growth & Design* **2017,** *17* (4), 2006-2015.
14. Carino, A.; Ludwig, C.; Cervellino, A.; Muller, E.; Testino, A., Formation and transformation of calcium phosphate phases under biologically relevant conditions: Experiments and modelling. *Acta Biomater* **2018,** *74*, 478-488.
15. Andalibi, M. R.; Wokaun, A.; Bowen, P.; Testino, A., Kinetics and Mechanism of Metal Nanoparticle Growth via Optical Extinction Spectroscopy and Computational Modeling: The Curious Case of Colloidal Gold. *ACS Nano* **2019,** *13* (10), 11510-11521.
16. Mohammed, A. S. A.; Carino, A.; Testino, A.; Andalibi, M. R.; Cervellino, A., In Situ Liquid SAXS Studies on the Early Stage of Calcium Carbonate Formation. *Part Part Syst Char* **2019,** *36* (6).
17. Gebauer, D.; Kellermeier, M.; Gale, J. D.; Bergstrom, L.; Colfen, H., Pre-nucleation clusters as solute precursors in crystallisation. *Chem Soc Rev* **2014,** *43* (7), 2348-71.
18. Dey, A.; Bomans, P. H.; Muller, F. A.; Will, J.; Frederik, P. M.; de With, G.; Sommerdijk, N. A., The role of prenucleation clusters in surface-induced calcium phosphate crystallization. *Nat Mater* **2010,** *9* (12), 1010-4.
19. Wang, L.; Li, S.; Ruiz-Agudo, E.; Putnis, C. V.; Putnisc, A., Posner's cluster revisited: direct imaging of nucleation and growth of nanoscale calcium phosphate clusters at the calcite-water interface *CrystEngComm* **2012,** *14*, 6252-6256
20. Zhang, Q.; Jiang, Y.; Gou, B.-D.; Huang, J.; Gao, Y.-X.; Zhao, J.-T.; Zheng, L.; Zhao, Y.-D.; Zhang, T.-L.; Wang, K., In Situ Detection of Calcium Phosphate Clusters in Solution and Wet Amorphous Phase by Synchrotron X□ray Absorption Near-Edge Spectroscopy at Calcium K□Edge. *Crystal Growth and Design* **2015,** *15*, 2204-2210.
21. Paul Tuck, S.; Layfield, R.; Walker, J.; Mekkayil, B.; Francis, R., Adult Paget's disease of bone: a review. *Rheumatology (Oxford)* **2017,** *56* (12), 2050-2059.
22. Ardenkjaer-Larsen, J. H.; Fridlund, B.; Gram, A.; Hansson, G.; Hansson, L.; Lerche, M. H.; Servin, R.; Thaning, M.; Golman, K., Increase in signal-to-noise ratio of > 10,000 times in liquid-state NMR. *Proc Natl Acad Sci* **2003,** *100* (18), 10158-63.
23. Kovtunov, K. V.; Pokochueva, E. V.; Salnikov, O. G.; Cousin, S. F.; Kurzbach, D.; Vuichoud, B.; Jannin, S.; Chekmenev, E. Y.; Goodson, B. M.; Barskiy, D. A.; Koptyug, I. V., Hyperpolarized NMR Spectroscopy: d-DNP, PHIP, and SABRE Techniques. *Chem Asian J* **2018**.
24. Jannin, S.; Dumez, J. N.; Giraudeau, P.; Kurzbach, D., Application and methodology of dissolution dynamic nuclear polarization in physical, chemical and biological contexts. *J Magn Reson* **2019,** *305*, 41-50.
25. Weber, E. M. M.; Sicoli, G.; Vezin, H.; Frébourg, G.; Abergel, D.; Bodenhausen, G.; Kurzbach, D., Sample Ripening through Nanophase Separation Influences the Performance of Dynamic Nuclear Polarization. *Angew. Chem. Int. Ed.* **2018**, 10.1002/anie.201800493.
26. Milani, J.; Vuichoud, B.; Bornet, A.; Mieville, P.; Mottier, R.; Jannin, S.; Bodenhausen, G., A magnetic tunnel to shelter hyperpolarized fluids. *Rev Sci Instrum* **2015,** *86* (2).
27. Miclet, E.; Abergel, D.; Bornet, A.; Milani, J.; Jannin, S.; Bodenhausen, G., Toward Quantitative Measurements of Enzyme Kinetics by Dissolution Dynamic Nuclear Polarization. *J Phys Chem Lett* **2014,** *5* (19), 3290-5.
28. Sadet, A.; Emmanuelle M. M. Weber; Jhajharia, A.; Kurzbach, D.; Bodenhausen, G.; Miclet, E.; Abergel, D., Kinetic rates of chemical metabolic processes determined by NMR boosted by dissolution dynamic nuclear polarization. *Chem. Eur. J.* **2018,** *24*, 5456 – 5461.
29. Ivanov, K. L.; Kress, T.; Guarin, D.; Baudin, M.; Abergel, D.; Bodenhausen, G.; Kurzbach, D., Relaxation of long-lived modes in NMR of deuterated methyl groups. *J. Chem. Phys.* **2018,** *149* (5), 054202.
30. Kress, T.; Walrant, A.; Bodenhausen, G.; Kurzbach, D., Long-Lived States in Hyperpolarized Deuterated Methyl Groups Reveal Weak Binding of Small Molecules to Proteins. *J Phys Chem Lett* **2019,** *10* (7), 1523-1529.
31. Stoll, S.; Schweiger, A., EasySpin, a comprehensive software package for spectral simulation and analysis in EPR. *J Magn Reson* **2006,** *178* (1), 42-55.
32. Castanar, L.; Poggetto, G. D.; Colbourne, A. A.; Morris, G. A.; Nilsson, M., The GNAT: A new tool for processing NMR data. *Magn Reson Chem* **2018,** *56* (6), 546-558.
33. Rothwell, W. P.; Waugh, J. S.; Yesinowski, J. P., High-resolution variable-temperature phosphorus-31 NMR of solid calcium phosphates. *J. Am. Chem. Soc.* **1980,** *102*, 2637-2673.
34. Nardi-Schreiber, A.; Gamliel, A.; Harris, T.; Sapir, G.; Sosna, J.; Gomori, J. M.; Katz-Brull, R., Biochemical phosphates observed using hyperpolarized 31P in physiological aqueous solutions. *Nat Commun* **2017,** *8* (1), 341.
35. Leon Swisher, C.; Koelsch, B.; Sukumar, S.; Sriram, R.; Santos, R. D.; Wang, Z. J.; Kurhanewicz, J.; Vigneron, D.; Larson, P., Dynamic UltraFast 2D EXchange SpectroscopY (UF-EXSY) of hyperpolarized substrates. *J Magn Reson* **2015,** *257*, 102-9.

36. Habraken, W. J., The integration of ion potentiometric measurements with chemical, structural, and morphological analysis to follow mineralization reactions in solution. *Methods Enzymol* **2013,** *532*, 25-44.
37. Costello, A. J. R.; Glonek, T.; Wazer, J. R. V., Phosphorus-31 Chemical Shift Variations with Countercation and Ionic Strength for the Various Ethyl Phosphates. *Inorg. Chem.* **1975,** *15*, 972-974.
38. Kurzbach, D.; Reh, M. N.; Hinderberger, D., Nanoscale inhomogeneities in thermoresponsive triblock copolymers. *Chemphyschem* **2011,** *12* (18), 3566-72.
39. Kurzbach, D.; Hassouneh, W.; McDaniel, J. R.; Jaumann, E. A.; Chilkoti, A.; Hinderberger, D., Hydration Layer Coupling and Cooperativity in Phase Behavior of Stimulus Responsive Peptide Polymers. *J Am Chem Soc* **2013,** *135* (30), 11299-11308.
40. Kurzbach, D.; Junk, M. J. N.; Hinderberger, D., Nanoscale Inhomogeneities in Thermoresponsive Polymers. *Macromol Rapid Commun* **2013,** *34* (2), 119-134.
41. Crutchfield, M. M.; Callis, C. V.; Irani, R. R.; Roth, G. C., Phosphorus Nuclear Magnetic Resonance Studies of Ortho and Condensed Phosphates. *Inorg. Chem.* **1962,** *1*, 813-817.
42. Wazer, J. R. V.; Callis, C. F.; Shoolery, J. N., NUCLEAR MAGNETIC RESONANCE SPECTRA OF THE CONDENSED PHOSPHATES. *J. Am. Chem. Soc.* **1955,** *77*, 4945-4956.